Proceedings of ICRC 2001: 861 © Copernicus Gesellschaft 2001

ICRC 2001

Simulated performance of the Orbiting Wide-angle Light collectors (OWL) experiment

J. F. Krizmanic[1,2] **and The OWL Collaboration**[3]

[1]Universities Space Research Association
[2]Laboratory for High Energy Astrophysics, NASA GSFC, Greenbelt, Maryland 20771 USA
[3]http://owl.gsfc.nasa.gov

Abstract. The Orbiting Wide-angle Light collectors (OWL) experiment is in NASA's mid-term strategic plan and will stereoscopically image, from equatorial orbit, the air fluorescence signal generated by airshowers induced by the ultra-high energy ($E >$ few $\times 10^{19}$ eV) component of the cosmic radiation. The use of a space-based platform enables an extremely large event acceptance aperture and thus will allow a high statistics measurement of these rare events. Detailed Monte Carlo simulations are required to quantify the physics potential of the mission as well as optimize the instrumental parameters. This paper reports on the results of the GSFC Monte Carlo simulation for two different, OWL instrument baseline designs. These results indicate that, assuming a continuation of the cosmic ray spectrum ($\phi \sim E^{-2.75}$), OWL could have an event rate of 4000 events/year with $E \geq 10^{20}$ eV. Preliminary results, based upon these Monte Carlo simulations, indicate that events can be accurately reconstructed in the detector focal plane arrays for the OWL instrument baseline designs under consideration.

1 Introduction

Cosmic rays with energies $> 10^{20}$ eV and thus above the Greisen-Zatsepin-Kuzmin (GZK) cutoff have been measured by numerous ground-based experiments (Nagano and Watson, 2000). The absence of obvious, nearby astrophysical sources of these events has created a mystery (Stecker, 2001) and has fueled an interest in developing experiments with the large aperture necessary to observe these extremely rare events with higher statistics (Cronin, 1999).

The OWL collaboration has been developing a space-based experiment (Krizmanic et al., 1998) to employ the air fluorescence technique to measure the airshowers induced by ultra-high energy (UHE) cosmic rays by employing stereoscopic imaging. Two satellites will monitor a large atmospheric volume and record the ultraviolet air fluorescence signals generated by the airshower with a time resolution of ~ 1 μs or less in segmented focal plane arrays. The segmentation of the arrays will be such as to sample the atmosphere near the Earth's surface in ~ 1 km^2 pixels and map the light signals into focal plane pixels where they are converted to an electrical signal. The measured trajectories of the imaged tracks in the focal plane detector arrays form the essential input to reconstruct the airshower in the atmosphere.

Inherent to the OWL development are Monte Carlo simulations which are necessary to understand the underlying physics and detail the response of orbiting instruments to the ultraviolet air fluorescence signals. One such Monte Carlo has been developed at GSFC (Krizmanic, 1999). The simulation employs a hadronic event generator that includes effects due to shower starting point and development fluctuations, charged pion decay, neutral pion re-interaction, and the Landau-Pomeranchuk-Migdal (LPM) effect (Mikulski, 2000). As the OWL baseline imaging requirements are rather insensitive to lateral shower size, the hadronic generator creates individual 1-dimensional shower parameterizations characterized by a 4-parameter Gaisser-Hillas function. Each airshower is developed in a sequence of fixed time intervals, $\delta t = 1$ μs for the results presented in this paper, and the resulting charged particles are used to generate wavelength-dependent air fluorescence (Bunner, 1967) and Cherenkov signals at the specific development point. The fluorescence signal is corrected for the pressure and temperature dependence of the atmosphere (Kakimoto et al., 1996). The pressure dependence assumes the Shibata parameterization (Gaisser, 1990), which is used to describe the altitude dependence of the atmosphere, while the 1976 U.S. Standard Atmosphere describes the atmospheric temperature profile. Large-angle scattering of the generated Cherenkov light, potentially into the viewing aperture of the instrument, is accounted for an angle-dependent scattering function (Baltrusaitis et al., 1985).

Once the ultraviolet light signal is generated, it must be propagated out of the atmosphere to the orbiting instruments. Two light-loss mechanisms are modeled, Rayleigh scattering

Correspondence to: J. F. Krizmanic
(jfk@cosmicra.gsfc.nasa.gov)

and ozone absorption (Krizmanic, 1999). The attenuation effects of the atmosphere are determined by calculating the slant depths of the atmosphere and ozone between the shower generation points and the orbiting instruments. The fluorescence and scattered Cherenkov signals are Rayleigh scattered with the scattered light assumed to be lost. Ozone losses are calculated using a low latitude ozone profile with a vertical column depth of 325 milliatm-cm. Effects due to aerosols and clouds are not considered for the study presented in this paper.

2 Instrument Modeling

Once the photons have been generated and propagated to the orbiting satellites, the response of the instruments to this signal can be modeled taking into account the wavelength dependence of the ultraviolet signal. Two different baseline instruments have been developed to achieve wide field-of-views (FOV's). The first is a refractive design which uses two Fresnel lenses which focus onto a large focal plane array (Lamb, 1998). The second design uses Fresnel correcting optics which focus onto an aspherical reflector in a Maksutov design which in turn focuses the light onto a focal plane array (Lamb, 1999; Pitalo, 2000). Response functions for the optical transmission and focal plane spot size as functions of shower viewing angle were developed for use in the simulation using the results of optical ray tracing modeling of each of the designs. The scale size of the optical elements in these designs are given in meters, and mechanical engineering studies have indicated they could be stowed in available rocket fairings and have straightforward deployment mechanisms.

2.1 Refractive Baseline Design

The Refractive baseline employs two Fresnel lenses focusing the collected light signal onto a large focal plane array. The effective optical aperture is 2.5 m in diameter with the optical elements sized larger and forming an f/#2.6 system. The design has a FOV of ± 30 degrees with an angular FOV of 0.1 deg for each 1×1 cm^2 pixel in the segmented focal plane array. The transmission of the optics as a function of viewing angle (θ) is parameterized by $T(\theta) = 0.842 - 0.817\theta^2 - 1.87\theta^4$ with θ given in radians. The reduction in transmission for the off-axis angles is due to the vignetting of the Fresnel lenses. An additional 5% transmission loss is assumed to account for material absorption losses. The light spot on the focal plane is approximated as a Gaussian distribution with a σ given by 0.45 cm on-axis ($\theta = 0$ deg) and decreases via a polynomial function to 0.38 cm at the maximum off-axis angle ($\theta = 30$ deg). The nominal orbits of the satellites in this configuration is set to be 640 km.

2.2 Maksutov Baseline Design

The Maksutov design incorporates two Fresnel correcting lenses which focus the incident light onto a large, aspherical reflector which directs the light onto a focal plane array. The optical aperture for this design in 3.5 m in diameter with the optical elements spanning a larger size and forming an f/#0.6 system. This design has a FOV of ± 25 deg and an angular FOV of 0.08 deg for each 3×3 mm^2 pixel in the focal plane array. The transmission as a function of viewing angle is given by $T(\theta) = 0.30 - 0.29\theta + 4.1\theta^2 - 4.1\theta^3$ with θ in radians. The on-axis transmission is significantly reduced in this design due to the obscuration of the focal plane array located up-stream of the reflector. An additional 5% transmission loss is assumed to account for material absorption losses. The light spot on the focal plane is approximated as a Gaussian distribution with a σ given by 0.3 mm on-axis ($\theta = 0$ deg) and increases via a parameterization to 1 mm at the maximum off-axis angle ($\theta = 25$ deg). The orbits are set to 1000 km for the results presented in this paper.

2.3 Focal Plane Array

Once the light transmission of the optical system is modeled, the light is further attenuating assuming the wavelength response of a BG-1 filter. The photon signal is then mapped onto the appropriate pixel of the focal plane array. This signal is spread to adjacent pixels assuming the appropriate pixel and Gaussian spot sizes for the instrument design being simulated. The photon signal in each pixel is integrated over the pixel size with the assumption of a 5% dead area located on the perimeter of each pixel. This is then convolved with the wavelength response of a bi-alkali photo-cathode, and the resultant pixel signals are Poisson fluctuated to obtain a photo-electron signal is each pixel for each time step.

3 Event Detection Aperture

The ability of the baseline designs in different configurations to detect cosmic rays can be expressed in terms of an aperture (km^2-ster) as a function of incident cosmic ray energy. The satellite configurations considered in this paper have both instruments orbiting at the same altitude, separated by a particular fixed distance, and tilted such that they view a common area on the Earth's surface. An event trigger is formed by setting a minimum criteria on the pixel hit distributions in each satellite. A photo-electron (PE) signal sum is formed by finding the pixel with the maximum PE signal in a particular time step and summing this signal and the signals in the nearest-neighbor pixels. For the aperture presented in this paper, a particular event is accepted if this sum is greater than 2 PE's in 5 or more time steps in each satellite. An isotropic flux of protons of a given incident energy is generated and the number of events accepted by the trigger condition is determined yielding an event trigger aperture for a given energy, instrument baseline, and satellite configuration.

Figure 1 illustrates the proton trigger aperture as a function of energy assuming the Refractive baseline and the satellites orbiting at 640 km. Two satellite separations are considered, 500 km and 2000 km. The figure demonstrates an increase

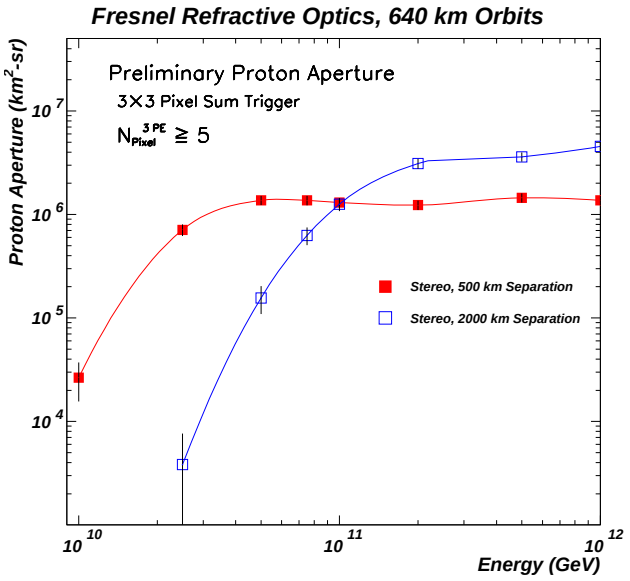

Fig. 1. The proton trigger aperture as a function of energy for the Refractive baseline design. The open squares are for a configuration with a satellite separation of 500 km while the closed squares are that for a 2000 km separation.

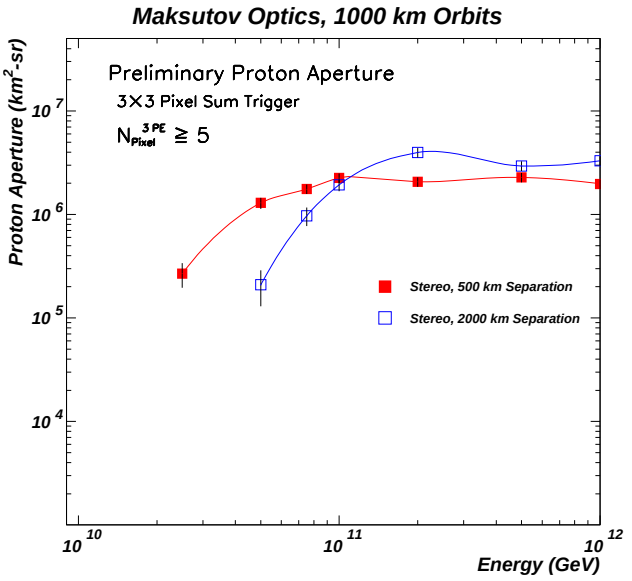

Fig. 2. The proton trigger aperture as a function of energy for the Maksutov baseline design. The open squares are for a configuration with a satellite separation of 500 km while the closed squares are that for a 2000 km separation.

in the asymptotic aperture as the separation distance is increased along with an increase in the threshold energy for event detection. These results reflect the differences in the configuration geometry. The 2000 km configuration has the instruments viewing a larger atmospheric volume while the events, on average, are a further distance from the satellites. The magnitude of the instantaneous apertures demonstrates the ability of the space-based methodology. For a satellite separation of 500 (2000) km, the instantaneous aperture is 1.5×10^6 (3.75×10^6) km^2-ster. Using a 10% duty factor, the 500 (2000) km separation configuration leads to an effective aperture of 1.5×10^5 (3.75×10^5) km^2-ster. Assuming a continuation of the cosmic ray spectrum as $\phi \sim E^{-2.75}$, these translate into event rates of 1500 events/year (500 km) and 3750 events/year (2000 km) for $E \geq 10^{20}$ eV.

The proton trigger aperture for the Maksutov baseline for 1000 km orbits is shown in Figure 2 for the configurations with 500 and 2000 km satellite separations. As in the previous case, the asymptotic aperture increases as the satellite separation is increased to 2000 km. Applying a 10% duty factor, the 500 km (2000 km) separation aperture is 2×10^5 (4×10^5) km^2-ster which leads to an event rate of 2000 (4000) events/year for $E \geq 10^{20}$ eV and a $\phi \sim E^{-2.75}$ spectrum continuation.

4 Event Reconstruction

Preliminary event reconstruction results using an early OWL design and a simulation based upon the HiRes experiment have been previously performed and demonstrated energy resolution of $< 15\%$ and good $X_{\rm Max}$ resolution for proton events with $E = 10^{20}$ eV (Dai et al., 1998). Results based upon an updated HiRes inspired simulation and event reconstruction will be presented at this conference (Abu-Zayyed, 2001). The event reconstruction based upon the GSFC simulation is at a preliminary stage, and the focal plane track fitting methodology is described here.

Figure 3 illustrates a 10^{20} eV proton event in each of the two OWL detector focal planes assuming the Maksutov baseline with the satellites orbiting at 1000 km and separated by 500 km. The figure shows the time-integrated signal over the entire event with the number of PE's given in each of the square, detector pixels. The total signal in one detector (Eye 1) is 265 PE's with a total, observed track length of 89 μs. The time-integrated signal in the second detector (Eye 2) is 255 PE's with an observed track length of 75 μsec. The transverse spread of the focal plane track is dominated by the spot size of the imaging optics.

A focal plane track fitting algorithm has been developed using a moment-of-inertia analysis of the time-integrated signal induced by an event in an individual focal plane. The algorithm treats the hit pixel distributions in each focal plane array as a 2-dimensional solid with the value of the PE signal in each pixel treated as a discrete mass point positioned at the center of each pixel. After the center-of-mass is calculated, the principal axes are determined by solving the eigenvalue problem. The axis of rotation corresponding to the smaller eigenvalue is taken to represent the image of the airshower track on the focal plane. This is constrained to pass through the center-of-mass and leads to a fit of the focal plane track.

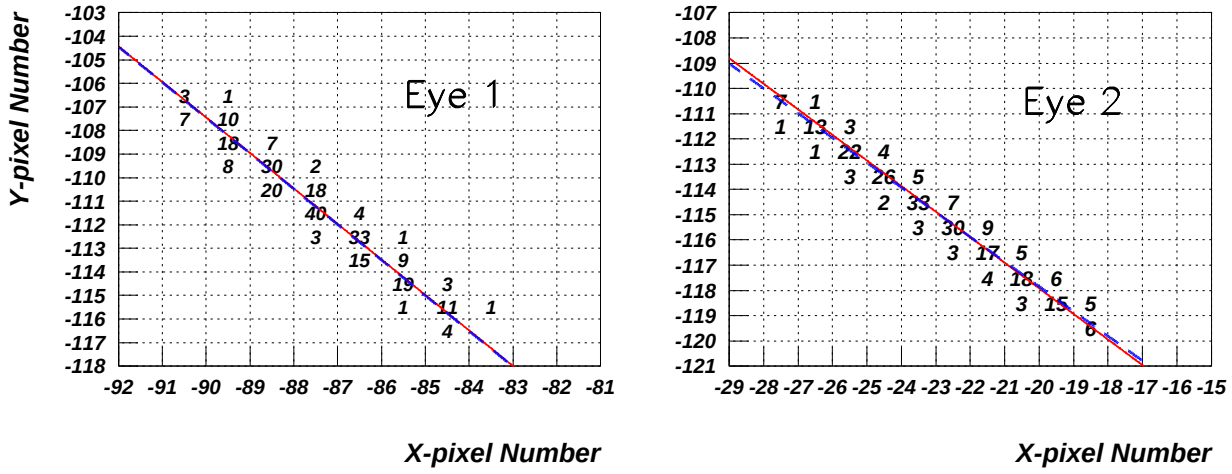

Fig. 3. The distribution of the photo-electrons in the focal planes for a 10^{20} eV proton event assuming the Maksutov baseline at 1000 km orbits. The number of photo-electrons in each pixel are denoted by the numbers in each plot. The blue, dashed line is the reconstructed fit of the event using a moment-of-inertia methodology. The red, solid line presents the actual track trajectories used in the Monte Carlo simulation.

The results of this fitting procedure for a particular event are shown in Figure 3 as the blue, dashed line in each focal plane view. This is to be compared to the red, solid lines which denotes the actual event trajectory in each focal plane which is provided by the Monte Carlo with infinite precision. The agreement between the reconstructed and actual tracks in the focal planes are quite good with the angles between the two lines less than 1 deg in each focal plane. The performance of the moment-of-inertia methodology demonstrates that the spread of the signal caused by the optic spot size can be accurately reconstructed using centroiding techniques.

References

Abu-Zayyed, T. and The OWL Collaboration, Event Reconstruction for the Orbiting Wide-angle Light collectors (OWL) Experiment Air-Fluorescence Detector, these proceedings, 2001

Baltrusaitis, R. et al., The Utah Fly's Eye Detector, Nucl. Inst. Meth., A240, 410–428,1985

Bunner, A., Cosmic Ray Detection by Atmospheric Fluorescence, Cornell University Ph.D. Thesis, 1967

Cronin, J., Cosmic Rays: The Most Energetic Particles in the Universe, Rev. Mod. Phys. 71, No. 2, S165–S172, 1999

Dai, H.Y., Loh, E.C., and Sokolsky, P., AIP Conf. Proc. 433, 382–389, 1998

Gaisser, T., Cosmic Rays and Particle Physics, Cambridge University Press, 1990

Kakimoto, F., Loh, E., Nagano, M., Okuno, H., Teshima, M., and Ueno, S., A Measurement of the Air Fluorescence Yield, Nucl. Inst. Meth., A372, 527–533,1996

Krizmanic, J.F., Performance of the Orbiting Wide-angle Light Collector (OWL/AirWatch) Experiment via Monte Carlo Simulation, 26th ICRC (Salt Lake City), 2-388–2-391, 1999

Krizmanic, J.F., Ormes, J.F., Streitmatter, R.E., The Proceedings of the Workshop on Observing Giant Cosmic Ray Airshowers from $> 10^{20}$ eV Particles from Space, AIP Conf. Proc. 433, 1998

Lamb, D., Chipman, R., Hillman, L., Takahashi, Y., and Dimmock, J., Wide Angle Refractive Optics for Astrophysical Applications, AIP Conf. Proc. 433, 428–433, 1998

Lamb, D., internal OWL Technical Note, 1999

Mikulski, P., Extensive Airshowers: Model Dependence and the Longitudinal Profile, Johns Hopkins University Ph.D. Thesis, 2000

Nagano, M. and Watson, A., Observations and Implications of the Ultrahigh-Energy Cosmic Rays, Rev.Mod.Phys.72, 689–732, 2000

Pitalo, K., internal OWL Technical Note, 2000

Stecker, F, The Curious Adventure of the Ultrahigh Energy Cosmic Rays, astro-ph/0101072, 2001